

pubs.acs.org/JACS Article

1D Hybrid Semiconductor Silver 2,6-Difluorophenylselenolate

Tomoaki Sakurada, Yeongsu Cho, Watcharaphol Paritmongkol, Woo Seok Lee, Ruomeng Wan, Annlin Su, Wenbi Shcherbakov-Wu, Peter Müller, Heather J. Kulik, and William A. Tisdale*



Cite This: J. Am. Chem. Soc. 2023, 145, 5183–5190



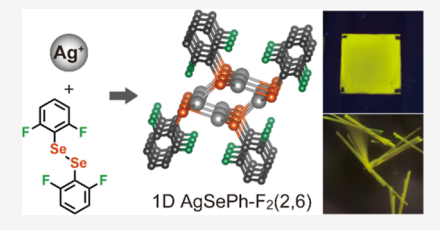
ACCESS

Metrics & More

Article Recommendations

s Supporting Information

ABSTRACT: Organic—inorganic hybrid materials present new opportunities for creating low-dimensional structures with unique light—matter interaction. In this work, we report a chemically robust yellow emissive one-dimensional (1D) semiconductor, silver 2,6-difluorophenylselenolate—AgSePhF $_2$ (2,6), a new member of the broader class of hybrid low-dimensional semiconductors, metal—organic chalcogenolates. While silver phenylselenolate (AgSePh) crystallizes as a two-dimensional (2D) van der Waals semiconductor, introduction of fluorine atoms at the (2,6) position of the phenyl ring induces a structural transition from 2D sheets to 1D chains. Density functional theory calculations reveal that



AgSePhF₂ (2,6) has strongly dispersive conduction and valence bands along the 1D crystal axis. Visible photoluminescence centered around $\lambda_{\rm p} \approx 570\,$ nm at room temperature exhibits both prompt (110 ps) and delayed (36 ns) components. The absorption spectrum exhibits excitonic resonances characteristic of low-dimensional hybrid semiconductors, with an exciton binding energy of approximately 170 meV as determined by temperature-dependent photoluminescence. The discovery of an emissive 1D silver organoselenolate highlights the structural and compositional richness of the chalcogenolate material family and provides new insights for molecular engineering of low-dimensional hybrid organic—inorganic semiconductors.

INTRODUCTION

Dimensional reduction of organic-inorganic hybrid semiconductors affords dynamic changes in optical, electronic, and vibrational properties. For example, transformation of bulk three-dimensional (3D) halide perovskites into two- (2D), one- (1D), or zero-dimensional (0D) perovskite structures through the modification of organic cations leads to increases in the electronic band gap and exciton binding energy through quantum and dielectric confinement effects. 2-4 Metal-organic chalcogenolates (MOCs) are another emerging family of lowdimensional hybrid materials, 5,6 finding applications as light emitters,^{7–15} field-effect transistors,^{16,17} photoconductors,^{14,18–20} photonic reflectors,²¹ and sensors.²² MOCs are distinguished from other low-dimensional semiconductors such as halide perovskites and transition metal chalcogenides by the covalent interaction between metals and organic ligands. Because of their covalent nature, MOCs are chemically stable, and hybridized inorganic-organic interaction in MOCs enables optoelectronic property tuning and morphology transformation via ligand modification. 5,23

A variety of MOCs from 0D to 1D to 2D have been synthesized by a combination of d^{10} coinage metals and organochalcogenolate ligands. Though the structure of MOCs is difficult to predict *a priori*, it is clear that interactions between ligands is a key factor. For example, phenylthiolate ligands form a 1D chain structure with copper (I) ions, ([CuSPh]_n), 16 while 2,4,6-triisopropylphenylthiolate, a bulkier ligand, leads to a 0D complex ([CuSC₆H₂(*i*-Pr)₃]₈). Helosh and co-workers synthesized Cu MOCs with bulky diamondoid ligands that behaved as 1D semiconductors. In another

example, Demessence and co-workers synthesized gold phenylthiolate derivatives with functional groups located at different positions of the benzene ring 10,11,26 and reported corresponding structural transformation from a 1D double helical chain of [AuSPh]_n to 2D lamellae of [Au(p-SPhCO₂H)]_n, induced by hydrogen bonding between neighboring mercaptobenzoic acid ligands. Dimensionality control can also induce dramatic changes in optoelectronic properties. Functional group modification of gold phenylthiolate MOCs led to increases in the photoluminescence quantum yield (PLQY) from 1 to 70%. Recently, silver phenylselenolate (AgSePh) was shown to be a 2D excitonic semiconductor exhibiting narrow deep-blue luminescence, inplane optical anisotropy, and chemical robustness. However, limited examples of structural modification in this promising new family of MOCs have been reported.

Here, we report structural modification of AgSePh through fluorination of the benzene ligand. Substituting phenylselenolate for 2,6-difluorophenylselenolate induced a structural transition from 2D AgSePh to 1D chain-structured silver 2,6-difluorophenylselenolate [AgSePh- $F_2(2,6)$]. Both crystals and films of AgSePh- $F_2(2,6)$ exhibited broad yellow luminescence. Crystals of AgSePh- $F_2(2,6)$ were stably emissive after soaking

Received: November 8, 2022 Published: February 22, 2023





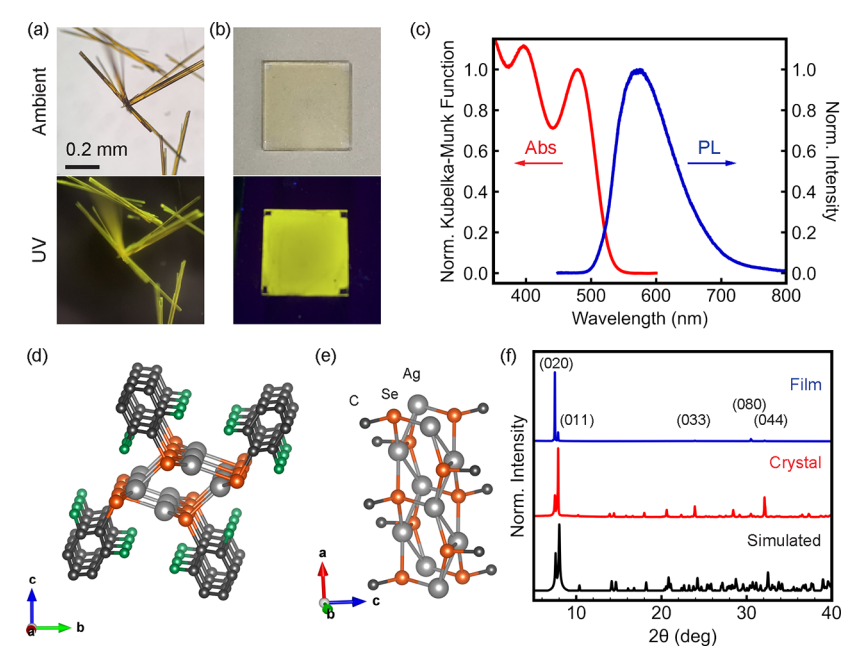


Figure 1. Optical micrograph and image of AgSePh- $F_2(2,6)$ (a) crystals and (b) film on a glass substrate (12 × 12 mm²) under ambient or UV (365 nm) light. (c) Absorption and PL spectra of AgSePh- $F_2(2,6)$ crystals. (d) Crystal structure of AgSePh- $F_2(2,6)$. Ag, Se, C, and F atoms are depicted by gray, orange, black, and green spheres, respectively. Hydrogen and disordered atoms are omitted for clarity. (e) Structure of the AgSe core in AgSePh- $F_2(2,6)$. (f) PXRD pattern of AgSePh- $F_2(2,6)$ in a film (blue), ground crystals (red), and a simulated (black) sample.

in various organic solvents and acidic or basic solutions. Electronic structural calculations reveal AgSePh- $F_2(2,6)$ to be a 1D semiconductor with light effective masses of holes $(0.20m_0)$ and electrons $(0.26m_0)$ at the band edge, suggesting its potential utility in electronic and optoelectronic devices. The emissive state is assigned to an exciton having a binding energy of approximately 170 meV, which can undergo entropically driven dissociation into free charge carriers along the 1D chain.

RESULTS AND DISCUSSION

To prepare AgSePh- $F_2(2,6)$, we first synthesized an organic precursor—1,2-bis(2,6-difluorophenyl) diselenide—by a reaction between an *in situ* prepared Grignard reagent, 2,6-difluorophenylmagnesium bromide, and elemental selenium (see the Supporting Information for more information).³⁰

Crystals of AgSePh-F₂(2,6) (Figure 1a) were synthesized using a water-diffusion-assisted growth method³¹ based on the previously reported amine-assisted crystallization.¹³ Briefly, a solution of silver nitrate (AgNO₃) and the organic diselenide precursor was prepared in a mixture of 1-butylamine and toluene (Figure S1b) and was filtered and transferred into a small vial sealed inside a larger jar containing deionized water (Figure S1c). Over time, deionized water and the mixed organic solvent were slowly exchanged, resulting in the lower solubility of AgSePh-F₂(2,6) and the formation of its submillimeter crystals that exhibited a needle-like shape (Figures 1a and S1d).

Thin films of AgSePh-F₂(2,6) (Figure 1b) were prepared by the conversion of metallic silver films via a vapor-phase chemical transformation known as the "tarnishing method". ^{8,14} A 5 nm thick silver film was deposited onto a glass substrate by thermal evaporation and then placed inside a microwave reaction vial containing the organic diselenide precursor and N_1N' -dimethylformamide (DMF). The vial was heated at 100

°C for 3 days, transforming the metallic silver film into a light-yellow film of AgSePh- $F_2(2,6)$ (Figure 1b).

Under UV light excitation, both crystals and films exhibited bright yellow emission, as shown in Figure 1a,b. The absorption spectrum of AgSePh- $F_2(2,6)$ displayed distinct peaks characteristic of low-dimensional excitonic semiconductors, with the lowest-energy absorption peak centered at 477 nm, as determined using UV—vis diffuse reflectance spectroscopy (Figure 1c). The emission spectrum of AgSePh- $F_2(2,6)$ exhibited broad yellow luminescence with a peak at 574 nm at room temperature (Figure 1c). The PLQY of sonicated dispersions of crystals in 2-propanol at room temperature was 2.4%.

Single crystal X-ray diffraction analysis at 100 K (Tables 1 and S1) revealed that AgSePh-F₂(2,6) forms a 1D hybrid organic-inorganic structure with an inorganic core composed of Ag and Se atoms surrounded by organic 2,6-difluorophenyl rings (Figure 1d). The core is composed of repeating Ag₄Se₄ units (Figure S2a) that each consist of two different Ag₂Se₂ parallelograms (Figure S2b,c) rotated in-plane by almost 90° with respect to each other and stacked along the direction of the 1D chain. The two different parallelograms are connected by four Ag-Se bonds and two argentophilic interactions (Figure 1e). The Ag-Se bond lengths range between 2.56 and 2.65 Å, and the separation of Ag atoms across planes is 2.99 and 3.20 Å, which is shorter than twice the van der Waals radius of a Ag atom (3.4 Å). 22 Each Se atom is connected by a covalent Se-C bond to a 2,6-difluorophenyl ring that points out in a perpendicular direction to the 1D chain.

The crystal structure of AgSePh-F₂(2,6) at 100 K shows evidence of both intra- and inter-chain interactions. Pairs of neighboring fluorobenzene ligands along the 1D chain have face-to-face distances of 3.28 to 3.30 Å (Figure S2d), suggesting an intra-chain π - π interaction.³³ Moreover, the presence of inter-chain hydrogen interactions between adjacent C-H···F-C bonds is suggested due to small H-F separations

Table 1. Crystallographic Data for AgSePh-F₂(2,6)

 $AgSePhF_2$ (2,6) identification code P21111 empirical formula C₆ H₃ Ag F₂ Se formula weight 299.91 temperature 100(2) K wavelength 0.71073 Å crystal system monoclinic $P2_1/n$ space group unit cell dimensions a = 4.62930(10) Åb = 23.2971(6) Åc = 12.5151(3) Å1348.62(6) Å³ volume density (calculated) 2.954 Mg/m³ 8.331 mm^{-1} absorption coefficient F(000) $0.250 \times 0.055 \times 0.015 \text{ mm}^3$ crystal size $\boldsymbol{\theta}$ range for data collection 1.748 to 33.200° $-7 \le h \le 7, -35 \le k \le 35, -19 \le l \le 19$ index ranges reflections collected 48566 independent reflections $5158 [R_{int} = 0.0310]$ completeness to θ = 25.242° 100.0% semi-empirical from equivalents absorption correction full-matrix least-squares on F^2 refinement method data/restraints/parameters 5158/453/236 goodness-of-fit on F2 final R indices $[I > 2\sigma(I)]$ R1 = 0.0180, wR2 = 0.0385R1 = 0.0218, wR2 = 0.0400R indices (all data)

of 2.42–2.75 Å (Figure S2e), which is in agreement with previous studies of other fluorobenzenes.³⁴

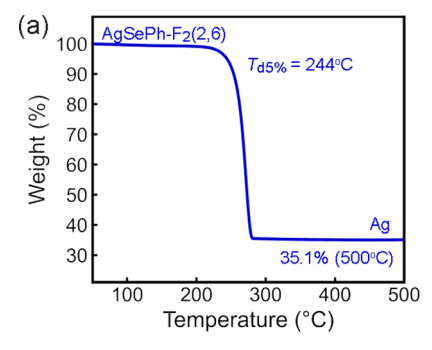
largest diff. peak and hole

2.292 and -0.645 e.Å-3

Unlike 2D van der Waals crystals of AgSePh, AgSePh- $F_2(2,6)$ exhibited a 1D chain structure. Quite recently, a few groups reported the ligand modification of 2D silver organochalcogenolates by *para*-substitution of the phenyl ring; ^{12,13,23} however, no significant structural change was observed in those studies. For AgSePh- $F_2(2,6)$, the distinct structural transformation may be induced by steric effects of fluorine atoms at the two *ortho*-positions, destabilizing the 2D sheet structure and forming a 1D chain to relax strain energy.

Powder X-ray diffraction (PXRD) analysis of ground crystals matched well with simulated data (Figure 1f). However, PXRD patterns collected on thin film samples selectively showed prominent (0k0) and (0kl) diffraction peaks, indicating a preference for crystal growth parallel to the substrate (Figures 1f and S3). Indeed, bright-field optical micrographs of thin film samples reveal needle like microcrystals of AgSePh-F₂(2,6) oriented parallel to the substrate (Figure S4), agreeing with PXRD data. No distinct peak from other chemicals was observed including the diffraction peak from Ag (\sim 38.2°). X-ray photoemission spectroscopy of the thin films of AgSePh-F₂(2,6) showed signal from Ag, Se, and F (Figure S5), with a Ag/Se ratio of 1:0.9, agreeing within the experimental error to the chemical formula of AgSePh-F₂(2,6).

AgSePh- $F_2(2,6)$ exhibited both thermal and chemical stability. Thermogravimetric analysis (TGA) revealed the stability of AgSePh- $F_2(2,6)$ up to ~200 °C under N_2 , with a 5% weight loss temperature of 244 °C (Figure 2a). The mass fraction remaining at 500 °C was 35.1%—equal to the mass fraction of Ag atoms in AgSePh- $F_2(2,6)$ (36.0%)—implying



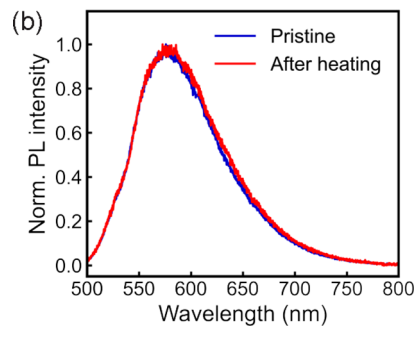


Figure 2. (a) TGA of AgSePh- $F_2(2,6)$ crystals under a N_2 flow. (b) PL spectrum of AgSePh- $F_2(2,6)$ crystals before (blue) and after heating (red) up to 100 °C under vacuum.

that silver was formed by thermolysis, as previously reported for 2D AgSePh. The PL spectra before and after heating up to 100 °C under vacuum were identical (Figure 2b), with some overall intensity loss. Furthermore, AgSePh- $F_2(2,6)$ is resistant to various organic solvents and can withstand both acidic and basic conditions. Crystals of AgSePh- $F_2(2,6)$ are insoluble and retain their luminescence properties even when submerged in polar organic solvents (N,N'-dimethylacetamide, DMF, acetonitrile, or methanol), a polar aromatic solvent (1,2-dichlorobenzene), or an acidic (pH = 1) or basic solution (pH = 14) (Figure S6). Strong chemical stability of AgSePh- $F_2(2,6)$ may originate from covalent bonding of the organoselenolate ligand to silver atoms along the 1D chain and from steric blocking of the silver selenide core by those ligands.

Density functional theory (DFT) calculations were performed to understand the electronic properties of AgSePh- $F_2(2,6)$. Figure 3a shows the calculated band structure of AgSePh- $F_2(2,6)$, having a direct band gap of 1.19 eV at Γ . The band structure is characteristic of 1D semiconductors with a large dispersion along the 1D chain and negligible dispersion along the other orthogonal axes (Figure 3a,b). The wave functions of the valence band maximum (VBM) and the conduction band minimum (CBM) at the Γ point are mostly located on the AgSe core (Figure 3c). The VBM of AgSePh- $F_2(2,6)$ mostly consists of Se 4p and Ag 4d orbitals, whereas the main contributions to the CBM are from Ag 5s and Se 4p orbitals (Figure S7). Both the band dispersion and the wave function distribution indicate that charge carriers near the Fermi level are highly confined in each chain and there is negligible hybridization between neighboring chains. Along the chain elongation $(\Gamma - X)$, the effective masses of the hole and electron are $0.20m_0$ and $0.26m_0$, respectively, where m_0 is the electron rest mass. These carrier effective masses are notably lighter than those reported in related 1D Cu MOC compounds (copper adamantane-1-thiolate and copper diadamantane-4thiolate), 25 which were close to or larger than $1m_0$.

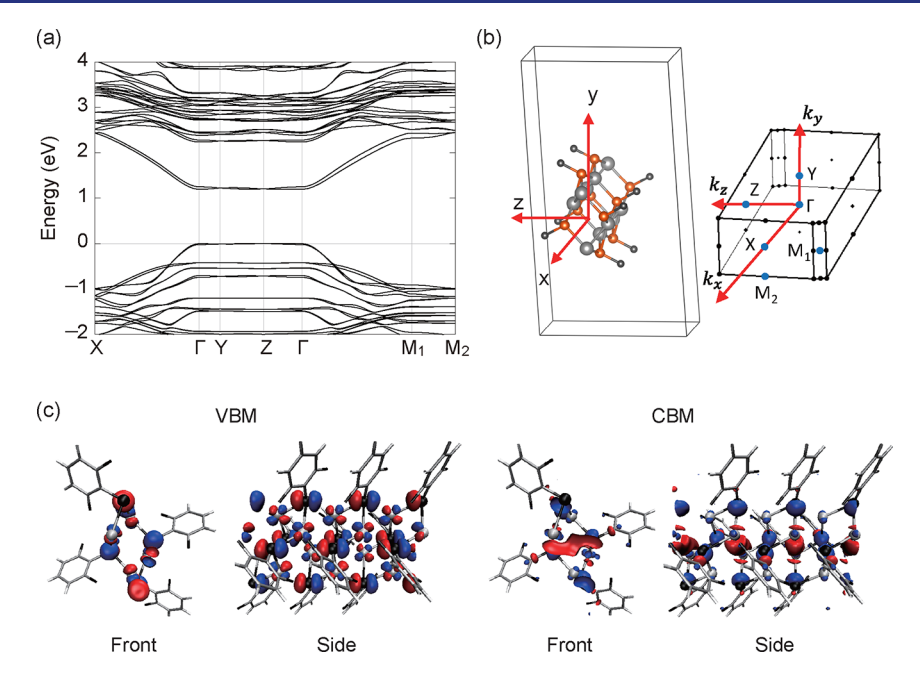


Figure 3. (a) Calculated electronic band structure of AgSePh-F₂(2,6). (b) First Brillouin zone with the corresponding atomic structures. k_x (Γ–X) is along the 1D chain; k_y and k_z are orthogonal to the 1D chain. (c) Wave functions of the VBM and the CBM at the Γ point, distributed within the silver selenide core.

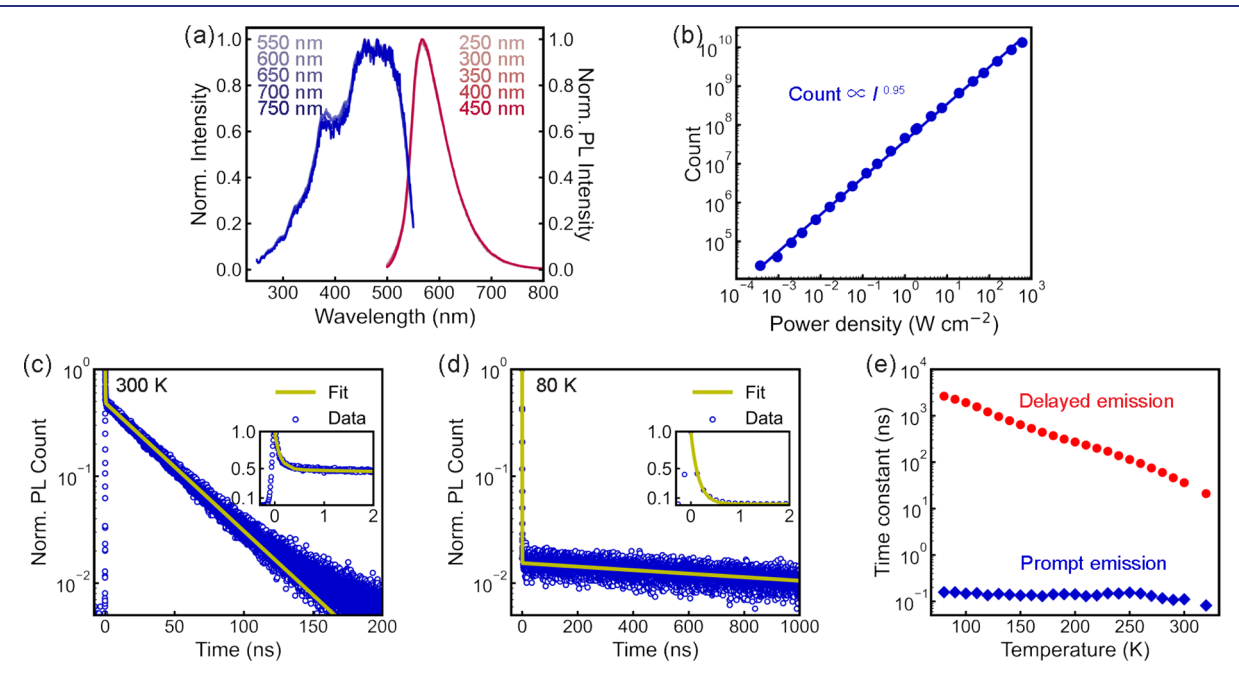


Figure 4. (a) PL excitation (blue, left) and emission (red, right) spectra of AgSePh- $F_2(2,6)$. (b) Plot of integrated PL count as a function of energy density of a continuous-wave laser (405 nm) with a range of 0.4 mW cm⁻² to 600 W cm⁻². TRPL decay and fit of AgSePh- $F_2(2,6)$ crystals at (c) 300 K and (d) 80 K. Insets show decay from a short time range. (e) Decay time of delayed (red) and prompt (blue) components obtained by bi-exponential fitting in the temperature range from 80 to 320 K.

To investigate light emission in AgSePh- $F_2(2,6)$, we measured PL properties upon exposure to different excitation wavelengths and different excitation intensities. No excitation or emission wavelength dependence was observed for PL spectra excited between 250–450 nm (Figure 4a, red) or PL excitation spectra with emission from 550–750 nm (Figure 4a, blue), indicating a single homogeneous emission pathway in the sample. Measurements of integrated PL emission intensities revealed linearly increasing PL intensity with increasing excitation laser power under both continuous-

wave (Figure 4b) and pulsed laser conditions (Figure S8). Similarly, the PL spectral shape was identical under low or high excitation power (Figure S9). The emission spectra of thin films and ground powders were similar to that of isolated crystals but with higher intensity in the 500 to 550 nm range, likely arising from inner-filter effects in the crystals (Figure S10). Altogether, these results suggest a single intrinsic and excitonic origin of the yellow emission of AgSePh-F₂(2,6).

Time-resolved PL (TRPL) decay of AgSePh- $F_2(2,6)$ was well-described by a bi-exponential function at all sample

temperatures across the measurement range from 80 to 320 K (Figures 4c,d and S11), with a fast prompt emission component that is more than 100× faster than the dominant delayed emission component (Figure 4e). As the sample was cooled below room temperature, the prompt decay slowed slightly from 110 ps at 300 K to 160 ps at 80 K, while the delayed component underwent a more dramatic change from 36 ns at 300 K to 2.6 μ s at 80 K (Figure 4e). The timeintegrated photon count ratio of prompt/delayed emission was 0.3:99.7, meaning that 99.7% of the total emission intensity occurs via the delayed emission channel. Despite the changing emission dynamics, the ratio of total photon counts from the prompt to delayed channels was approximately constant across the temperature range (Table S2). The PL spectrum was also measured from 80 to 300 K (Figure 5c). The spectrum blueshifted with increasing temperature from 615 nm (2.02 eV) at 80 K to 574 nm (2.16 eV) at 300 K.

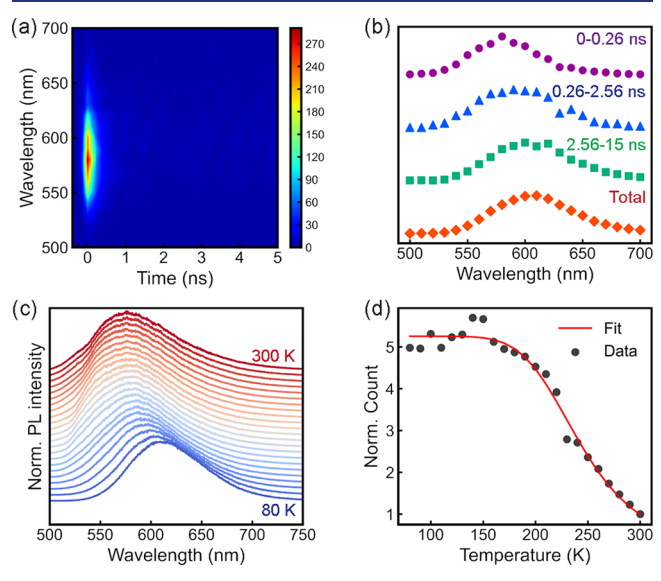


Figure 5. (a) Spectrally resolved TRPL spectrum of AgSePh-F₂(2,6) crystals at 80 K. (b) PL spectrum of AgSePh-F₂(2,6) crystals at 80 K from 0 to 0.26 ns (purple), 0.26 to 2.56 ns (blue), and 2.56 to 15 ns (green) and the total count (red). The time window from 0 to 0.26 ns (purple) is dominated by the prompt emission pathway (97%), whereas the time window from 2.56 to 15 ns (green) is dominated by the delayed emission pathway (~100%). (c) Normalized PL spectra of AgSePh- $F_2(2,6)$ in the temperature range of 80 to 300 K. (d) Temperature dependence of PL intensity from 80 to 300 K.

To further understand the emission dynamics, we performed spectrally resolved TRPL at 80 K (Figure 5a), which allows the emission spectrum of the prompt and delayed components to be separately analyzed. The PL spectrum collected during the 0 to 0.26 ns time window, which is dominated by prompt emission, had a peak wavelength of 570 nm (Figure 5b, purple). The PL spectrum collected during the 2.56 to 15 ns time window, which is derived ~100% from the delayed component, had a peak wavelength of 610 nm (Figure 5b, green). The total emission spectrum (Figure 5b, red) is nearly identical to the delayed emission spectrum, agreeing with our earlier calculation that ~99.7% of the total emission occurs through the delayed emission channel.

There are multiple hypotheses that could explain the prompt and delayed emission behavior. As shown by spectrally resolved TRPL (Figure 5b), the prompt and delayed emission

spectra are close in energy. A similar behavior has been observed in CdSe nanoplatelets, which was attributed to radiative recombination before and after exciton dissociation.³ In that case, the delayed emission originates from electronhole pairs that have dissociated then later re-formed an emissive exciton and the slight red shift at the later times arises from energetic heterogeneity within the sample. An alternative hypothesis is thermally activated delayed fluorescence (TADF).³⁷ A variety of Ag complexes³⁸ including multinuclear Ag complexes²⁷ have been reported as TADF emitters with a high PLQY. Under the TADF hypothesis, the slight red shift at later times could result from contributions of phosphorescence to the measured signal. Finally, band-edge excitons in low-dimensional semiconductors can exhibit a complicated fine structure ^{39–41} due to exchange, spin–orbit, shape, and crystal field effects, in which case, contributions from both exciton dissociation and spin-flip transitions could affect the measured emission dynamics.

As temperature increased, the total integrated PL intensity decreased (Figure 5d and Table S3). Assuming one thermally activated nonradiative recombination pathway, the temperature-dependent emission intensity can be well-fitted by the Arrhenius equation $(eq 1)^{42}$

$$I(T) = \frac{I_0}{1 + A \exp\left(\frac{-E_a}{k_B T}\right)} \tag{1}$$

where I(T) is the integrated PL count at temperature T, I_0 is the integrated intensity at a temperature approaching 0 K, A is a process rate parameter, Ea is the activation energy for nonradiative decay, and $k_{\rm B}$ is the Boltzmann constant. Fitting to the Arrhenius equation gives $E_a = 166 \pm 13$ meV (Figure 5d

The temperature-dependent emission behavior shown in Figure 5d is characteristic of low-dimensional excitonic semiconductors, where the dominant non-radiative recombination pathway is exciton dissociation followed by nonradiative relaxation of the separated charge carriers. 2,43,44 Under this interpretation, the activation energy is the thermal energy required to separate the electron-hole pair, i.e., the exciton binding energy. Correspondingly, we assign the exciton binding energy in AgSePh-F₂(2,6) to be $E_b \approx 170$ meV. Note that even though $E_b > k_B T$ at room temperature, exciton dissociation can still proceed efficiently due to strong entropic driving forces arising from the highly dispersive conduction and valence bands.4

CONCLUSIONS

In conclusion, we presented a yellow luminescent 1D silver organoselenolate using 2,6-difluorophenyl selenolate as a ligand. Introducing fluorine atoms at the two ortho-positions induced structural transformation from 2D van der Waals crystals of AgSePh to 1D chain structured AgSePh-F₂(2,6). AgSePh-F₂(2,6) exhibited thermal and chemical stability, and both DFT calculations and optical spectroscopy reveal an excitonic 1D semiconductor with strongly dispersive conduction and valence bands along the 1D chain.

The discovery of a new 1D member of the promising silver phenylchalcogenolate family of semiconducting MOCs encourages further exploration of this attractive molecular design space. Furthermore, the strongly excitonic nature of the electronic excited state in AgSePh-F₂(2,6) suggests its potential

use in a variety of optoelectronic applications featuring anisotropic conductors or emitters.

ASSOCIATED CONTENT

Supporting Information

The Supporting Information is available free of charge at https://pubs.acs.org/doi/10.1021/jacs.2c11896.

Combined X-ray crystallographic information of Ag-SePh- $F_2(2,6)$, experimental details, experimental data, spectra, schematics, and additional crystallographic information of AgSePh- $F_2(2,6)$ (PDF)

Accession Codes

CCDC 2204375–2204376 contain the supplementary crystallographic data for this paper. These data can be obtained free of charge via www.ccdc.cam.ac.uk/data_request/cif, or by emailing data_request/cif, or by contacting The Cambridge Crystallographic Data Centre, 12 Union Road, Cambridge CB2 1EZ, UK; fax: +44 1223 336033.

AUTHOR INFORMATION

Corresponding Author

William A. Tisdale — Department of Chemical Engineering, Massachusetts Institute of Technology, Cambridge, Massachusetts 02139, United States; oorcid.org/0000-0002-6615-5342; Email: tisdale@mit.edu

Authors

Tomoaki Sakurada — Department of Chemical Engineering, Massachusetts Institute of Technology, Cambridge, Massachusetts 02139, United States; Present Address: Yokohama technical center, AGC Inc., Suehiro 1-1, Tsurumi, Yokohama, Kanagawa, 230-0045, Japan; orcid.org/0000-0002-2353-7324

Yeongsu Cho — Department of Chemical Engineering, Massachusetts Institute of Technology, Cambridge, Massachusetts 02139, United States; orcid.org/0000-0001-8159-600X

Watcharaphol Paritmongkol – Department of Chemical Engineering, Massachusetts Institute of Technology, Cambridge, Massachusetts 02139, United States; Department of Chemistry, Massachusetts Institute of Technology, Cambridge, Massachusetts 02139, United States; orcid.org/0000-0003-1638-6828

Woo Seok Lee – Department of Chemical Engineering, Massachusetts Institute of Technology, Cambridge, Massachusetts 02139, United States; Department of Materials Science and Engineering, Massachusetts Institute of Technology, Cambridge, Massachusetts 02139, United States; orcid.org/0000-0001-9188-5104

Ruomeng Wan — Department of Chemical Engineering, Massachusetts Institute of Technology, Cambridge, Massachusetts 02139, United States; Department of Chemistry, Massachusetts Institute of Technology, Cambridge, Massachusetts 02139, United States

Annlin Su — Department of Chemical Engineering, Massachusetts Institute of Technology, Cambridge, Massachusetts 02139, United States

Wenbi Shcherbakov-Wu — Department of Chemical Engineering, Massachusetts Institute of Technology, Cambridge, Massachusetts 02139, United States; Department of Chemistry, Massachusetts Institute of Technology, Cambridge, Massachusetts 02139, United States Peter Müller — Department of Chemistry, Massachusetts Institute of Technology, Cambridge, Massachusetts 02139, United States; oorcid.org/0000-0001-6530-3852

Heather J. Kulik – Department of Chemical Engineering, Massachusetts Institute of Technology, Cambridge, Massachusetts 02139, United States; Department of Chemistry, Massachusetts Institute of Technology, Cambridge, Massachusetts 02139, United States; orcid.org/0000-0001-9342-0191

Complete contact information is available at: https://pubs.acs.org/10.1021/jacs.2c11896

Author Contributions

All authors discussed the results and reviewed the manuscript.

The authors declare no competing financial interest. All available data are included in the main article and the Supporting Information.

ACKNOWLEDGMENTS

Synthesis and structural characterization were supported by the U.S. Army Research Office under Award Number W911NF-20-1-0200. Optical spectroscopy was supported by the U.S. Department of Energy, Office of Science, Basic Energy Sciences, under award number DE-SC0019345. The electronic structure calculations were supported in part by the United States Department of Energy under grant number DE-NA0003965. We thank Baston and Prof. Yuriy Román-Leshkov for support and assistance with TGA measurement. T.S. acknowledges the support from AGC Inc. W.S.L was partially supported by the Seoul Broadcasting System Foundation Overseas Doctoral Program Scholarship.

REFERENCES

- (1) Tulsky, E. G.; Long, J. R. Dimensional Reduction: A Practical Formalism for Manipulating Solid Structures. *Chem. Mater.* **2001**, *13*, 1149–1166.
- (2) Manser, J. S.; Christians, J. A.; Kamat, P. V. Intriguing Optoelectronic Properties of Metal Halide Perovskites. *Chem. Rev.* **2016**, *116*, 12956–13008.
- (3) Dey, A.; Ye, J.; De, A.; Debroye, E.; Ha, S. K.; Bladt, E.; Kshirsagar, A. S.; Wang, Z.; Yin, J.; Wang, Y.; Quan, L. N.; Yan, F.; Gao, M.; Li, X.; Shamsi, J.; Debnath, T.; Cao, M.; Scheel, M. A.; Kumar, S.; Steele, J. A.; Gerhard, M.; Chouhan, L.; Xu, K.; Wu, X.; Li, Y.; Zhang, Y.; Dutta, A.; Han, C.; Vincon, I.; Rogach, A. L.; Nag, A.; Samanta, A.; Korgel, B. A.; Shih, C.-J.; Gamelin, D. R.; Son, D. H.; Zeng, H.; Zhong, H.; Sun, H.; Demir, H. V.; Scheblykin, I. G.; Mora-Seró, I.; Stolarczyk, J. K.; Zhang, J. Z.; Feldmann, J.; Hofkens, J.; Luther, J. M.; Pérez-Prieto, J.; Li, L.; Manna, L.; Bodnarchuk, M. I.; Kovalenko, M. V.; Roeffaers, M. B. J.; Pradhan, N.; Mohammed, O. F.; Bakr, O. M.; Yang, P.; Müller-Buschbaum, P.; Kamat, P. V.; Bao, Q.; Zhang, Q.; Krahne, R.; Galian, R. E.; Stranks, S. D.; Bals, S.; Biju, V.; Tisdale, W. A.; Yan, Y.; Hoye, R. L. Z.; Polavarapu, L. State of the Art and Prospects for Halide Perovskite Nanocrystals. ACS Nano 2021, 15, 10775–10981.
- (4) Han, Y.; Yue, S.; Cui, B.-B. Low-Dimensional Metal Halide Perovskite Crystal Materials: Structure Strategies and Luminescence Applications. *Sci. Adv.* **2021**, *8*, 2004805.
- (5) Veselska, O.; Demessence, A. d¹⁰ Coinage Metal Organic Chalcogenolates: From Oligomers to Coordination Polymers. *Coord. Chem. Rev.* **2018**, 355, 240.
- (6) Wang, G.-E.; Luo, S. Z.; Di, T.; Fu, Z. H.; Xu, G. Layered Organic Metal Chalcogenides (OMCs): From Bulk to Two-Dimensional Materials. *Angew. Chem., Int. Ed.* **2022**, 61, No. e202203151.

- (7) Schriber, E. A.; Popple, D. C.; Yeung, M.; Brady, M. A.; Corlett, S. A.; Hohman, J. N. Mithrene Is a Self-Assembling Robustly Blue Luminescent Metal—Organic Chalcogenolate Assembly for 2D Optoelectronic Applications. *ACS Appl. Nano Mater.* **2018**, *1*, 3498—3508.
- (8) Trang, B.; Yeung, M.; Popple, D. C.; Schriber, E. A.; Brady, M. A.; Kuykendall, T. R.; Hohman, J. N. Tarnishing Silver Metal into Mithrene. J. Am. Chem. Soc. 2018, 140, 13892–13903.
- (9) Maserati, L.; Refaely-Abramson, S.; Kastl, C.; Chen, C. T.; Borys, N. J.; Eisler, C. N.; Collins, M. S.; Smidt, T. E.; Barnard, E. S.; Strasbourg, M.; Schriber, E. A.; Shevitski, B.; Yao, K.; Hohman, J. N.; Schuck, P. J.; Aloni, S.; Neaton, J. B.; Schwartzberg, A. M. Anisotropic 2D Excitons Unveiled in Organic—Inorganic Quantum Wells. *Mater. Horiz.* **2021**, *8*, 197–208.
- (10) Lavenn, C.; Guillou, N.; Monge, M.; Podbevšek, D.; Ledoux, G.; Fateeva, A.; Demessence, A. Shedding Light on an Ultra-Bright Photoluminescent Lamellar Gold Thiolate Coordination Polymer [Au(p-SPhCO₂Me)]_n. Chem. Commun. **2016**, 52, 9063–9066.
- (11) Veselska, O.; Guillou, N.; Ledoux, G.; Huang, C.-C.; Dohnalova Newell, K.; Elkaïm, E.; Fateeva, A.; Demessence, A. A New Lamellar Gold Thiolate Coordination Polymer, [Au(m-SPhCO₂H)]_n, for the Formation of Luminescent Polymer Composites. *Nanomaterials* **2019**, *9*, 1408.
- (12) Yao, K.; Collins, M. S.; Nell, K. M.; Barnard, E. S.; Borys, N. J.; Kuykendall, T.; Hohman, J. N.; Schuck, P. J. Strongly Quantum-Confined Blue-Emitting Excitons in Chemically Configurable Multiquantum Wells. *ACS Nano* **2021**, *15*, 4085–4092.
- (13) Paritmongkol, W.; Sakurada, T.; Lee, W. S.; Wan, R.; Müller, P.; Tisdale, W. A. Size and Quality Enhancement of 2D Semiconducting Metal—Organic Chalcogenolates by Amine Addition. *J. Am. Chem. Soc.* **2021**, *143*, 20256–20263.
- (14) Paritmongkol, W.; Lee, W. S.; Shcherbakov-Wu, W.; Ha, S. K.; Sakurada, T.; Oh, S. J.; Tisdale, W. A. Morphological Control of 2D Hybrid Organic–Inorganic Semiconductor AgSePh. ACS Nano 2022, 16, 2054–2065.
- (15) Lee, W. S.; Cho, Y.; Powers, E. R.; Paritmongkol, W.; Sakurada, T.; Kulik, H. J.; Tisdale, W. A. Light Emission in 2D Silver Phenylchalcogenolates. *ACS Nano* **2022**, *16*, 20318–20328.
- (16) Che, C.-M.; Li, C.-H.; Chui, S. S.-Y.; Roy, V. a. L.; Low, K.-H. Homoleptic Copper(I) Arylthiolates as a New Class of p-Type Charge Carriers: Structures and Charge Mobility Studies. *Chem.—Eur J.* 2008, 14, 2965–2975.
- (17) Low, K.-H.; Li, C.-H.; Roy, V. A. L.; Chui, S. S.-Y.; Chan, S. L.-F.; Che, C.-M. Homoleptic Copper(I) Phenylselenolate Polymer as a Single-Source Precursor for Cu₂Se Nanocrystals. Structure, Photoluminescence and Application in Field-Effect Transistor. *Chem. Sci.* **2010**, *1*, 515–518.
- (18) Huang, Q.-Q.; Li, Y.-Z.; Zheng, Z.; Jiang, X.-M.; Sun, S.-S.; Jiang, H.-J.; Deng, W.-H.; Wang, G.-E.; Zhai, T.-Y.; Li, M.-D.; Xu, G. Single-Component MLCT-Active Photodetecting Material Based on a Two-Dimensional Coordination Polymer. CCS Chem. 2020, 2, 655–662
- (19) Maserati, L.; Prato, M.; Pecorario, S.; Passarella, B.; Perinot, A.; Thomas, A. A.; Melloni, F.; Natali, D.; Caironi, M. Photo-Electrical Properties of 2D Quantum Confined Metal—Organic Chalcogenide Nanocrystal Films. *Nanoscale* **2021**, *13*, 233–241.
- (20) Liu, G.-N.; Xu, R.-D.; Li, M.-K.; Sun, Y.; Zhou, M.-J.; Cai, R.-Y.; You, Z.-J.; Jiang, X.-M.; Li, C. Ultrathin Covalent and Cuprophilic Interaction-Assembled Copper—Sulfur Monolayer in Organic Metal Chalcogenide for Oriented Photoconductivity. *Chem. Commun.* **2022**, *58*, 2858–2861.
- (21) Wu, Z.; Yao, Q.; Liu, Z.; Xu, H.; Guo, P.; Liu, L.; Han, Y.; Zhang, K.; Lu, Z.; Li, X.; Zhang, J.; Xie, J. Multiscale Assembly of [AgS₄] Tetrahedrons into Hierarchical Ag–S Networks for Robust Photonic Water. *Adv. Mater.* **2021**, *33*, 2006459.
- (22) Jiang, H.; Cao, L.; Li, Y.; Li, W.; Ye, X.; Deng, W.; Jiang, X.; Wang, G.; Xu, G. Organic "Receptor" Fully Covered Few-Layer Organic—Metal Chalcogenides for High-Performance Chemiresistive

- Gas Sensing at Room Temperature. Chem. Commun. 2020, 56, 5366-5369.
- (23) Li, Y.; Jiang, X.; Fu, Z.; Huang, Q.; Wang, G.-E.; Deng, W.-H.; Wang, C.; Li, Z.; Yin, W.; Chen, B.; Xu, G. Coordination Assembly of 2D Ordered Organic Metal Chalcogenides with Widely Tunable Electronic Band Gaps. *Nat. Commun.* **2020**, *11*, 261.
- (24) Haas, A.; Schinkel, K. Synthese und chemische Eigenschaften von Pentafluorbenzolselenonsäure und Derivatisierung der Trifluormethanselenonsäure. *Chem. Ber.* **1990**, *123*, 685–689.
- (25) Yan, H.; Hohman, J. N.; Li, F. H.; Jia, C.; Solis-Ibarra, D.; Wu, B.; Dahl, J. E. P.; Carlson, R. M. K.; Tkachenko, B. A.; Fokin, A. A.; Schreiner, P. R.; Vailionis, A.; Kim, T. R.; Devereaux, T. P.; Shen, Z.-X.; Melosh, N. A. Hybrid Metal—Organic Chalcogenide Nanowires with Electrically Conductive Inorganic Core through Diamondoid-Directed Assembly. *Nat. Mater.* 2017, 16, 349—355.
- (26) Lavenn, C.; Okhrimenko, L.; Guillou, N.; Monge, M.; Ledoux, G.; Dujardin, C.; Chiriac, R.; Fateeva, A.; Demessence, A. A Luminescent Double Helical Gold(I)—Thiophenolate Coordination Polymer Obtained by Hydrothermal Synthesis or by Thermal Solid-State Amorphous-to-Crystalline Isomerization. *J. Mater. Chem. C* 2015, 3, 4115–4125.
- (27) Han, Z.; Dong, X.-Y.; Luo, P.; Li, S.; Wang, Z.-Y.; Zang, S.-Q.; Mak, T. C. W. Ultrastable Atomically Precise Chiral Silver Clusters with More than 95% Quantum Efficiency. *Sci. Adv.* **2020**, *6*, No. eaay0107.
- (28) Schriber, E. A.; Paley, D. W.; Bolotovsky, R.; Rosenberg, D. J.; Sierra, R. G.; Aquila, A.; Mendez, D.; Poitevin, F.; Blaschke, J. P.; Bhowmick, A.; Kelly, R. P.; Hunter, M.; Hayes, B.; Popple, D. C.; Yeung, M.; Pareja-Rivera, C.; Lisova, S.; Tono, K.; Sugahara, M.; Owada, S.; Kuykendall, T.; Yao, K.; Schuck, P. J.; Solis-Ibarra, D.; Sauter, N. K.; Brewster, A. S.; Hohman, J. N. Chemical Crystallography by Serial Femtosecond X-Ray Diffraction. *Nature* 2022, 601, 360–365.
- (29) Veselska, O.; Dessal, C.; Melizi, S.; Guillou, N.; Podbevšek, D.; Ledoux, G.; Elkaim, E.; Fateeva, A.; Demessence, A. New Lamellar Silver Thiolate Coordination Polymers with Tunable Photoluminescence Energies by Metal Substitution. *Inorg. Chem.* **2019**, *58*, 99–105.
- (30) Reich, H. J.; Renga, J. M.; Reich, I. L. Organoselenium Chemistry. Conversion of Ketones to Enones by Selenoxide Syn Elimination. *J. Am. Chem. Soc.* 1975, 97, 5434–5447.
- (31) Müller, P. Practical Suggestions for Better Crystal Structures. *Crystallogr. Rev.* **2009**, *15*, 57–83.
- (32) Bondi, A. Van Der Waals Volumes and Radii. *J. Phys. Chem.* **1964**, *68*, 441–451.
- (33) Tsuzuki, S.; Honda, K.; Uchimaru, T.; Mikami, M.; Tanabe, K. Origin of Attraction and Directionality of the π/π Interaction: Model Chemistry Calculations of Benzene Dimer Interaction. *J. Am. Chem. Soc.* **2002**, *124*, 104–112.
- (34) Thalladi, V. R.; Weiss, H.-C.; Bläser, D.; Boese, R.; Nangia, A.; Desiraju, G. R. C–H···F Interactions in the Crystal Structures of Some Fluorobenzenes. *J. Am. Chem. Soc.* **1998**, *120*, 8702–8710.
- (35) Popple, D. C.; Schriber, E. A.; Yeung, M.; Hohman, J. N. Competing Roles of Crystallization and Degradation of a Metal—Organic Chalcogenolate Assembly under Biphasic Solvothermal Conditions. *Langmuir* **2018**, *34*, 14265.
- (36) Rabouw, F. T.; van der Bok, J. C.; Spinicelli, P.; Mahler, B.; Nasilowski, M.; Pedetti, S.; Dubertret, B.; Vanmaekelbergh, D. Temporary Charge Carrier Separation Dominates the Photoluminescence Decay Dynamics of Colloidal CdSe Nanoplatelets. *Nano Lett.* **2016**, *16*, 2047–2053.
- (37) Yang, Z.; Mao, Z.; Xie, Z.; Zhang, Y.; Liu, S.; Zhao, J.; Xu, J.; Chi, Z.; Aldred, M. P. Recent Advances in Organic Thermally Activated Delayed Fluorescence Materials. *Chem. Soc. Rev.* **2017**, *46*, 915–1016.
- (38) Yersin, H.; Czerwieniec, R.; Shafikov, M. Z.; Suleymanova, A. F. TADF Material Design: Photophysical Background and Case Studies Focusing on CuI and AgI Complexes. *ChemPhysChem* **2017**, *18*, 3508–3535.

- (39) Norris, D. J.; Efros, Al. L.; Rosen, M.; Bawendi, M. G. Size Dependence of Exciton Fine Structure in CdSe Quantum Dots. *Phys. Rev. B* **1996**, *53*, 16347–16354.
- (40) Becker, M. A.; Vaxenburg, R.; Nedelcu, G.; Sercel, P. C.; Shabaev, A.; Mehl, M. J.; Michopoulos, J. G.; Lambrakos, S. G.; Bernstein, N.; Lyons, J. L.; Stöferle, T.; Mahrt, R. F.; Kovalenko, M. V.; Norris, D. J.; Rainò, G.; Efros, A. L. Bright Triplet Excitons in Caesium Lead Halide Perovskites. *Nature* **2018**, *553*, 189–193.
- (41) Posmyk, K.; Zawadzka, N.; Dyksik, M.; Surrente, A.; Maude, D. K.; Kazimierczuk, T.; Babiński, A.; Molas, M. R.; Paritmongkol, W.; Mączka, M.; Tisdale, W. A.; Płochocka, P.; Baranowski, M. Quantification of Exciton Fine Structure Splitting in a Two-Dimensional Perovskite Compound. *J. Phys. Chem. Lett.* **2022**, *13*, 4463–4469.
- (42) Lambkin, J. D.; Considine, L.; Walsh, S.; O'Connor, G. M.; McDonagh, C. J.; Glynn, T. J. Temperature Dependence of the Photoluminescence Intensity of Ordered and Disordered In_{0.48}Ga_{0.52}P. *Appl. Phys. Lett.* **1994**, *65*, 73–75.
- (43) Mauck, C. M.; Tisdale, W. A. Excitons in 2D Organic-Inorganic Halide Perovskites. *Trends Chem.* **2019**, *1*, 380.
- (44) Amori, A. R.; Hou, Z.; Krauss, T. D. Excitons in Single-Walled Carbon Nanotubes and Their Dynamics. *Annu. Rev. Phys. Chem.* **2018**, *69*, 81.
- (45) Gélvez-Rueda, M. C.; Hutter, E. M.; Cao, D. H.; Renaud, N.; Stoumpos, C. C.; Hupp, J. T.; Savenije, T. J.; Kanatzidis, M. G.; Grozema, F. C. Interconversion between Free Charges and Bound Excitons in 2D Hybrid Lead Halide Perovskites. *J. Phys. Chem.* C 2017, 121, 26566–26574.

☐ Recommended by ACS

Bottom-Up Synthesis of Metalated Carbyne Ribbons via Elimination Reactions

Wenze Gao, Wei Xu, et al.

MARCH 10, 2023

JOURNAL OF THE AMERICAN CHEMICAL SOCIETY

READ 🗹

Electronic Structure and Excited State Dynamics of Cadmium Chalcogenide Nanorods

Katherine E. Shulenberger, Gordana Dukovic, et al.

MARCH 07, 2023

CHEMICAL REVIEWS

READ 🗹

Light Emission in 2D Silver Phenylchalcogenolates

Woo Seok Lee, William A. Tisdale, et al.

NOVEMBER 23, 2022

ACS NANO

READ 🗹

A Free Phosphaborene Stable at Room Temperature

Jiancheng Li, Liu Leo Liu, et al.

DECEMBER 15, 2022

JOURNAL OF THE AMERICAN CHEMICAL SOCIETY

READ 🗹

Get More Suggestions >